Journal of
Materials Chemistry C

Improving the efficiencies of small molecule solar cells by solvent vapor annealing to enhance the J-aggregation

SCHOLARONE™
Manuscripts

Improving the efficiencies of small molecule solar cells by solvent vapor annealing to enhance the J-aggregation

Liangang Xiao[abc], Zhengdong Li[a], Qin Hu[de], Yawei Liu[c], Wenkai Zhong[b], Xueli Mei[f], Thomas P. Russell[de], Yi Liu*[c], Yong Min[a], Xiaobin Peng*[b] and Yong Cao[b]

a. School of Materials and Energy, Guangdong University of Technology, Guangzhou 510006, China

b. State Key Laboratory of Luminescent Materials and Devices, Institute of Polymer Optoelectronic Materials and Devices, South China University of Technology, 381 Wushan Road, Guangzhou 510640, China

c. The Molecular Foundry, Lawrence Berkeley National Lab, Berkeley, CA, 94720, United States

d. Materials Sciences Division, Lawrence Berkeley National Lab, Berkeley, CA, 94720, United States

e. Polymer Science and Engineering Department, University of Massachusetts, Amherst, MA 01003, United States

f. College of Chemistry, Chemical Engineering and Material Science of Soochow University, Suzhou, Jiangsu, 215123, China

Abstract: We report highly efficient small molecule organic solar cells (SM-OSCs) based on a porphyrin derivative electron donor of ZnP2-DPP and an electron acceptor of [6,6]-phenyl-C61-butyric acid methyl ester ($PC_{60}BM$) by using solvent vapor annealing (SVA) method with a series of low boiling solvents. Absorption spectra study indicate that carbon disulfide (CS_2) SVA induce J-aggregation in blend films accompanied with expanded and enhanced absorptions which contribute largely to fabricate broader light response and larger short-circuit current (J_{SC}) solar cell devices. In addition, we systematically analyze the relationship between film morphology and device performance. Finally, the electronic study shows that the CS_2 SVA-treated device obtained higher exciton generation rate and carrier collection efficiency. And the morphology study indicates that the blend film treated by CS_2

SVA exhibits tighter molecular packing, better crystallization and appropriate phase separation length scale. In a word, these collective electronic and morphological features correlate well with the champion J_{SC}, fill factor (FF) and power conversion efficiency (PCE) for the CS_2 treated devices.

Keywords: J-aggregation, morphological features, solvent vapor annealing, small molecule solar cells

Introduction

Advances in material science have contributed to the development of clean energy production and energy storage technologies, as well as to the improvement of the ecological environment.[1-4] Bulk-heterojunction (BHJ) organic solar cells (OSCs) are very promising alternative to inorganic devices in generating low-cost renewable energy.[5-8] Small molecule photovoltaic donor materials have attracted much attention due to their many advantages of easier purification, well-defined molecular structures and less batch-to-batch variation compared to their polymer donor counterparts.[9-12] Recent progresses in material design, the optimization of device structures and enhanced morphology control have made the power conversion efficiency (PCE) of solution processed BHJ small molecules organic solar cells (SM-OSCs) more than 10%.[13-17] However, The PCEs of most SM-OSCs are still lower than those of polymer cells because of the limited understanding of the morphology control and manipulating on the fabrication of active layers. As we know, the exciton generation and separation, and carrier transportation and collection taken place inside the active layer are largely responsible for the device performance. Some fabrication processing such as additive processing, thermal annealing (TA) and solvent vapor annealing (SVA) are effective in changing the molecular crystallization and orientation and controlling the phase separation, domain size and domain purity of active layers. For examples, Heeger et al., reported SM-OSCs based on a small molecule 5,5'-bis((4-(7-hexylthiophen-2-yl)thiophen-2-yl)-[1,2,5]thiadiazolo[3,4-c]pyridine)-3,

3'-di-2-ethylhexylsilylene-2,2'-bithiophene (DTS(PTTh$_2$)$_2$). The PCE was enhanced from 4.5% to 6.7% and the nano-morphology of the domains of the blend films decreased from 20-30 nm dimensions to 15-20 nm in size when using 1,8-diiodooctane (DIO) as the additive.[18] Wang et al., reported multifluorine substituted oligomer BIT6F-based SM-OSCs with a PCE of 9.09% when the active layer was treated by TA+SVA. The performance enhancement was because the crystalline content and phase separation increased after SVA or TA + SVA treatment which allowed the molecules to move and order.[19]

Of all optimization methods known to influence the morphology of an active layer, SVA treatments are regarded as being especially efficient to SM-OSCs. In SVA treatment, active layer is exposed in a container saturated with solvent vapor. And the solvent vapor can diffuse into the blends and drastically lower the glass transition temperatures of the materials, and thus the molecules in the blends gain high mobility to reorganize into lower energy states.[20, 21] As a result, it could change the molecular crystallization and orientation, promote the aggregation of both donor and acceptor molecules. The improved phase purity and the increased phase separation length scale to a suitable state are beneficial to better device performance.[22, 23]

For organic conjugated molecules, the expansion of π-conjugation could enhance self-aggregation through intermolecular π-π interactions. Inter-chain Coulombic interactions of molecule assemblies always lead to H-aggregates, whereas intra-chain through-bond interactions lead to J-aggregates.[24, 25] Compared with the absorption in solution, the blue-shift of a film's absorption indicates that the molecule prefers H-aggregation. And a J-aggregation always refers an ordered molecule packing in one dimension and results in significant red-shift absorption with increased intensity.[26-28] And the expanded and enhanced absorptions in J-aggregation-based films provide the potential chance to fabricate broader light response and larger short-circuit current (J_{SC}) solar cell devices.
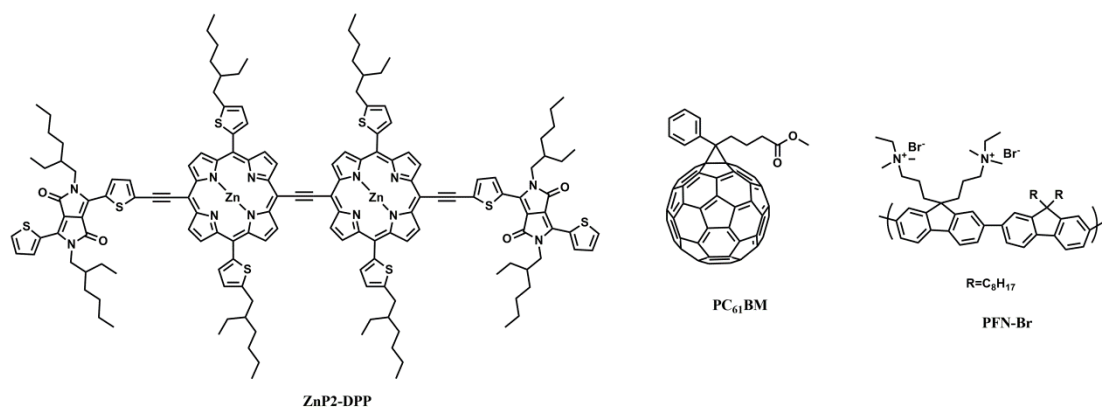
Figure 1. Chemical structures of ZnP2-DPP, PC$_{61}$BM and PFN-Br.

Some of porphyrin derivatives are near-infrared (NIR) organic semiconductors with optical bandgap less than 1.5 eV which have attracted much attention due to their great contribution to the field of NIR photodetector,[29, 30] SM-OSCs,[31-41] ternary solar cells[42-46] and tandem solar cells.[47, 48] In this contribution, we report dimer porphyrin molecule ZnP2-DPP [49] (Figure 1) based SM-OSCs and use SVA treatment with chloroform (CF), dichloromethane (CH$_2$Cl$_2$), carbon disulfide (CS$_2$) or tetrahydrofuran (THF) to control the thin film morphology and the optimize charge transport. The optimized devices show a high power conversion efficiency of 9.47% with an open-circuit voltage (V_{OC}) of 0.64 V, a fill factor (FF) of 69.14% and an impressively high J_{SC} of 21.40 mA cm^{-2} due to the strong absorption beyond 1000 nm of J-aggregation features induced by CS$_2$ SVA. The electronic study shows that the CS$_2$ SVA-treated device obtained higher exciton generation rate and carrier collection efficiency. And the morphology study indicates that the blend film treated by CS$_2$ SVA exhibits tighter molecular packing, better crystallization and appropriate phase separation length scale.
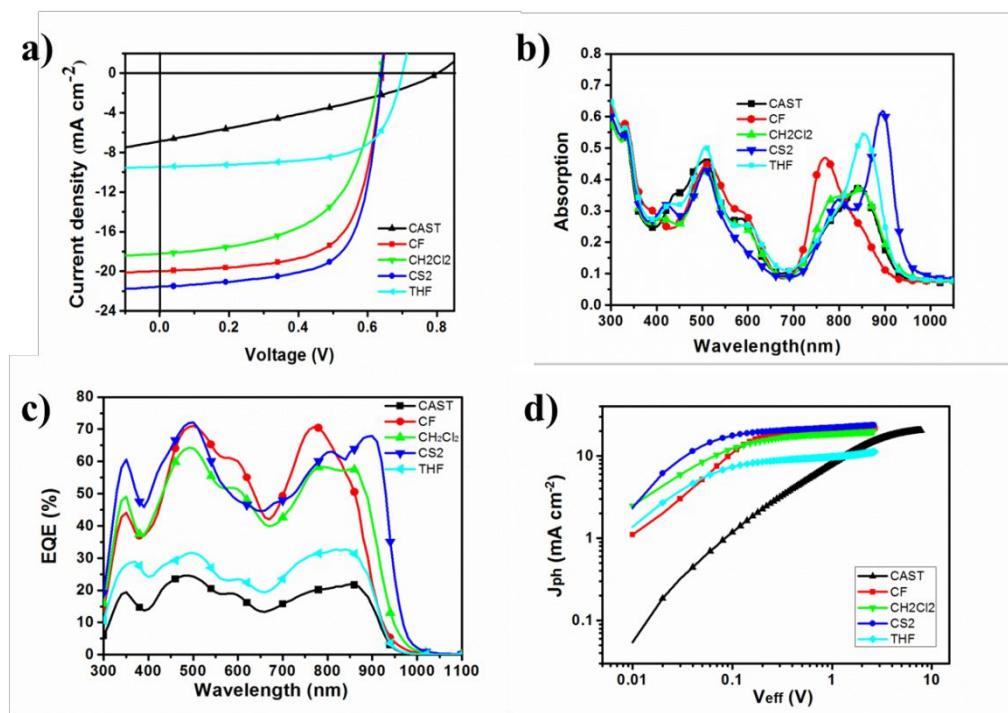
Results and discussion

Figure 2. a) The *J-V* curves of the solar cells; b) the absorption spectra of the blend films); c) the EQE curves of the solar cells; d) the photocurrent density versus effective voltage curves of the solar cells based on ZnP2-DPP:PC$_{61}$BM under different solvent vapor annealing processing conditions.

The SM-OSCs were fabricated with a conventional structure of ITO/PEDOT:PSS/ZnP2-DPP:PC$_{61}$BM/PFN-Br/Al. (PFN-Br: poly[(9,9-bis(3′-((*N*,*N*-dimethyl)-*N*-ethylammonium)-propyl)-2,7-fluorene)-*alt*-2,7-(9,9-di octylfluorene)]dibromide).[50] The fabricating process is shown in supporting information. Figure 2a shows the *J-V* curve of the solar cell devices with or without SVA and the corresponding photovoltaic parameters are shown in Table 1 and S1-S4. For the device based on the as-cast film, the *J$_{SC}$* and FF are extremely low, leading to an inferior efficiency of only 1.70%. Surprisingly, the *J$_{SC}$* and FF are obviously improved for all the SVA treated devices. Due to the low *J$_{SC}$* of 9.47 mA cm^{-2}, THF treated devices show a moderate PCE of 4.42% despite of its high *FF* of 66.20% and *V$_{OC}$* of 0.705 V. And for the devices treated with CH$_2$Cl$_2$, the *J$_{SC}$* is dramatically enhanced to 18.20 mA cm^{-2}. Unfortunately, the FF of the device is still less than 60%, which limited the improvement of PCE. For the devices treated with CF or CS$_2$, the

FF and PCE of the both devices exceed 67% and 8%, respectively. Especially, the champion PCE of 9.47% is obtained with an impressive J_{SC} of 21.40 mA cm^{-2}, a high FF of 69.14% and a V_{OC} of 0.64 V.

Table 1. Photovoltaic parameters for ZnP2-DPP:PC$_{61}$BM-based solar cells with different solvent vapor annealing processing conditions.

SVA	J_{SC} (mA cm^{-2})	V_{OC} (V)	FF (%)	PCE(%)
CAST	6.88 (6.58)[a]	0.805	31.02	1.70[b] (1.60)[c]
CF	19.85 (19.23)[a]	0.640	67.04	8.52[b] (8.36)[c]
CH$_2$Cl$_2$	18.20 (17.72)[a]	0.635	57.36	6.63[b] (6.50)[c]
CS$_2$	21.40 (20.52)[a]	0.640	69.14	9.47[b] (9.22)[c]
THF	9.47 (9.11)[a]	0.705	66.20	4.42[b] (4.32)[c]

a) J_{SC} calculated from EQE curve; b) the best PCE; c) average PCE from ten devices.

In order to understand the big differences of J_{SC} and PCE of these devices, we measured the absorption spectra and external quantum efficiency (EQE) spectra. The absorption of this molecule in solution shows a narrow peak in 789 nm and the absorption in as-cast film show a peak at 844 nm with an obvious red-shift of 55 nm, indicating good stacking and self-assembly properties of ZnP2-DPP (Figure S1). We used ZnP2-DPP and PC$_{61}$BM at the weight ratio of 1:1 to make active layer of solar cells. When preparing the blend films under different solvent vapor annealing process, there are big differences in the films' color which can be easily recognized by naked eyes, indicating that the absorption of these films change significantly after treated by different solvents. Indeed, as shown in Figure 2b, while the CH$_2$Cl$_2$ SVA treated film shows an absorption peak at the same position of 844 nm as that of the as-cast film, an apparent shoulder peak can be seen at 795 nm. For the blend film treated by CS$_2$ SVA, the maximum absorption peak dramatically red-shifts to 896 nm and the absorption shoulder in the 795 nm become more obvious. Such a broad absorption is beneficial for the solar cell devices to absorb more sunlight, resulting in a larger

photocurrent. Compared with that of the as-cast film, the absorption of THF SVA treated film only exhibits a moderate red-shift of 11 nm to 855nm. On the contrary, for the film treated with CF SVA, this absorption peak blue-shifts to 768 nm, which is even blue-shifted compared with the absorption in the solution (Figure S2). Such a blue-shift is generally considered as H-aggregation, which shall be attributed to the parallel alignment of the molecular dipole moments.[51, 52]

The EQE curves of the solar cells based on different solvent treatment are shown in Figure 2c. Obviously, the as-cast device and the THF-treated device show weak light response in the whole region possibly because of the well-mix of the donor and the acceptor and the severe phase separation length scale (*vide infra*). The EQE values of other three devices enhanced significantly and the shapes of the EQE curves are similar to their corresponding films absorption. The EQE curve of the CS_2-treated device show significant red shift when compared to the curve of CF-treated device. The integrated current density from the EQE curve is 20.52 mA/cm^2, which is similar with the measured value.

Single carrier devices were fabricated with the structure of ITO/PEDOT:PSS/ ZnP2-DPP:$PC_{61}BM$/MoO_3/Al. And the dark *J-V* curves of the devices under different SVA treatment were measured to evaluate the hole mobility using the space-charge limited current (SCLC) method, which are shown in Figure S3 and Table S5. While the as-cast device shows a low hole mobility of 1.65×10^{-5} cm^2 V^{-1} s^{-1},THF and CH_2Cl_2 SVA treatments improve the hole mobilities of the devices to 3.01×10^{-5} and 8.07×10^{-5} cm^2 V^{-1} s^{-1} , respectively. Especially, CF and CS_2 treated devices exhibited the higher mobilities of 1.50×10^{-4} cm^2 V^{-1} s^{-1} and 1.76×10^{-4} cm^2 V^{-1} s^{-1}, respectively, which can contribute to the high J_{SC} and FF of devices.

Photocurrent density (J_{ph}) is plotted against the effective voltage (V_{eff}) to investigate the exciton dissociation and charge collection efficiency of the cells.[53, 54] As showed in Figure 2d, CS_2 treated device shows the highest J_{ph} in low V_{eff}, indicating the best carrier collection efficiency. J_{ph} will be saturated (J_{sat}) when the V_{eff} is large enough. The maximum exciton generation rate (G_{max}) of the solar cells can be calculated according to the equation $J_{sat}=qLG_{max}$, where q is elementary charge,

L is the thickness of the active layer. The G_{max} values for the CF and CS$_2$ treated devices are 1.33×10^{28} m^{-3} s^{-1} and 1.46×10^{28} m^{-3} s^{-1}, respectively. Higher G_{max} derived from forming J-aggregation to enhance and broaden absorption induced by CS$_2$ SVA.

The surface morphology of the pristine and different solvent vapor annealing ZnP2-DPP:PC$_{61}$BM blend thin films is investigated by tapping-mode atomic force microscopy (AFM), and the images are shown in Figure S4. The root-mean-square (RMS) roughness values of the blend films with CF, CH$_2$Cl$_2$, CS$_2$ and THF SVA are 1.13, 0.41, 3.74 and 2.01 nm, respectively. In contrast, the as-cast film shows very smooth surface with a RMS of only 0.28 nm, indicating the extremely well mix of the porphyrin donor and the acceptor, which can lead to severe charge recombination and therefore a low FF because effective carrier transportation channel doesn't form. For the film treated with CF SVA, the surface roughness is obviously increased to 1.13 nm. And there were obvious aggregations with RMS of 2.01 nm in THF SVA treatment film. In particular, CS$_2$ vapor treated film shows a rougher surface and characteristic fiber-like structures can be seen clearly in height image, which might due to favorable crystalline of porphyrin molecules.
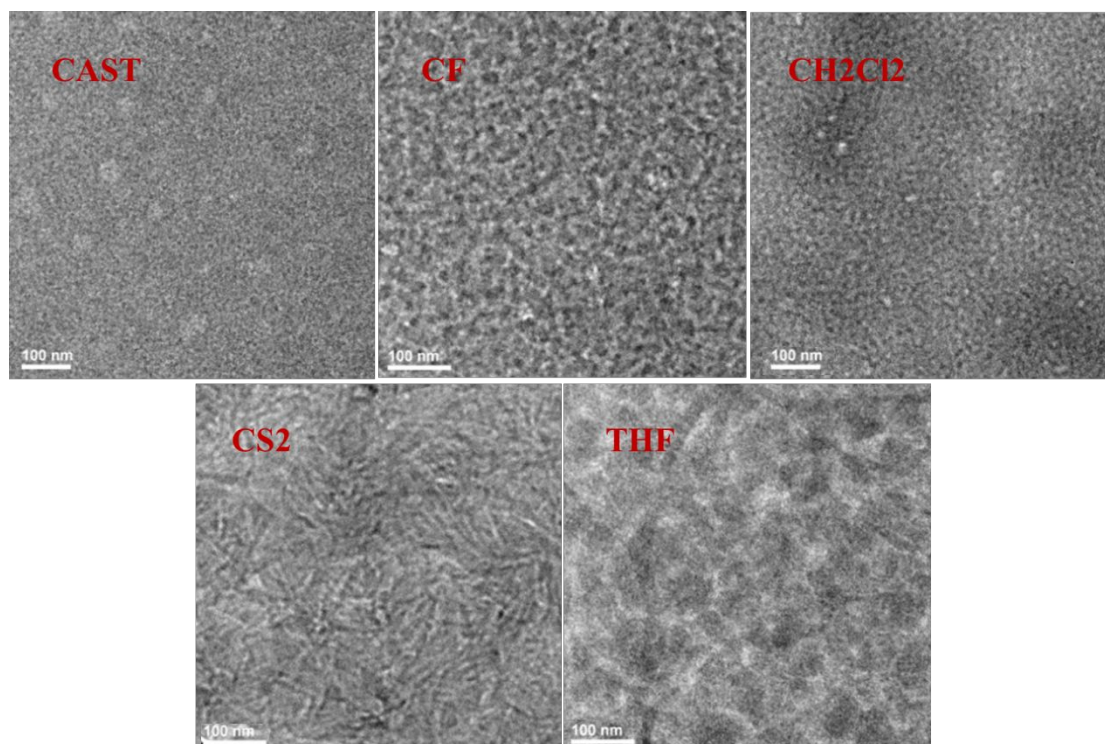

Figure 3. TEM images of ZnP2-DPP:PC$_{61}$BM blend films under different solvent

vapor annealing.

In order to obtain more information on the nanoscale phase separation, transmission electron microscopy (TEM) of ZnP2-DPP:$PC_{61}BM$ blend thin films spin-coated on ITO/PEDOT:PSS substrates with different solvent vapor annealing processing conditions is performed and the corresponding images are shown in Figure 3. The bright domains are ZnP2-DPP rich and the dark domains are $PC_{61}BM$ rich. A homogeneous morphology with unapparent nano-scale phase separation is seen for the as-cast film. Upon solvent vapor annealing, both the uniform mixture morphology and the length scale of phase separation are totally changed and the films display quite different surface morphology. Worm-like structures can be seen in the CF vapor annealing treated films, which is beneficial for exciton diffusion to the donor-acceptor interface and the concomitant exciton dissociation. For CH_2Cl_2 vapor treated film, length scale of phase separation is slightly enlarged and there are no well-defined domains. In particular, CS_2 SVA treated film shows obvious fiber-like structures in the TEM image. Apparently, the formation of fiber-like structures is in line with the absorption investigation that J-aggregation is enhanced in the blends upon CS_2 treatment, Well-defined morphology and suitable phase separation forming superior interpenetrating networks can contribute to the high charge transportation and therefore photovoltaic performance. It is no doubt that the solar cells treated by CS_2 vapor annealing display the highest FF of 69.14% and the largest PCE of 9.47%. However, obvious $PC_{61}BM$ dark domains larger than 100 nm appear in the THF SVA treatment films. The lack of D/A interfaces for separating excitons leads to a low current density of 9.47 mA cm^{-2} for the corresponding devices.
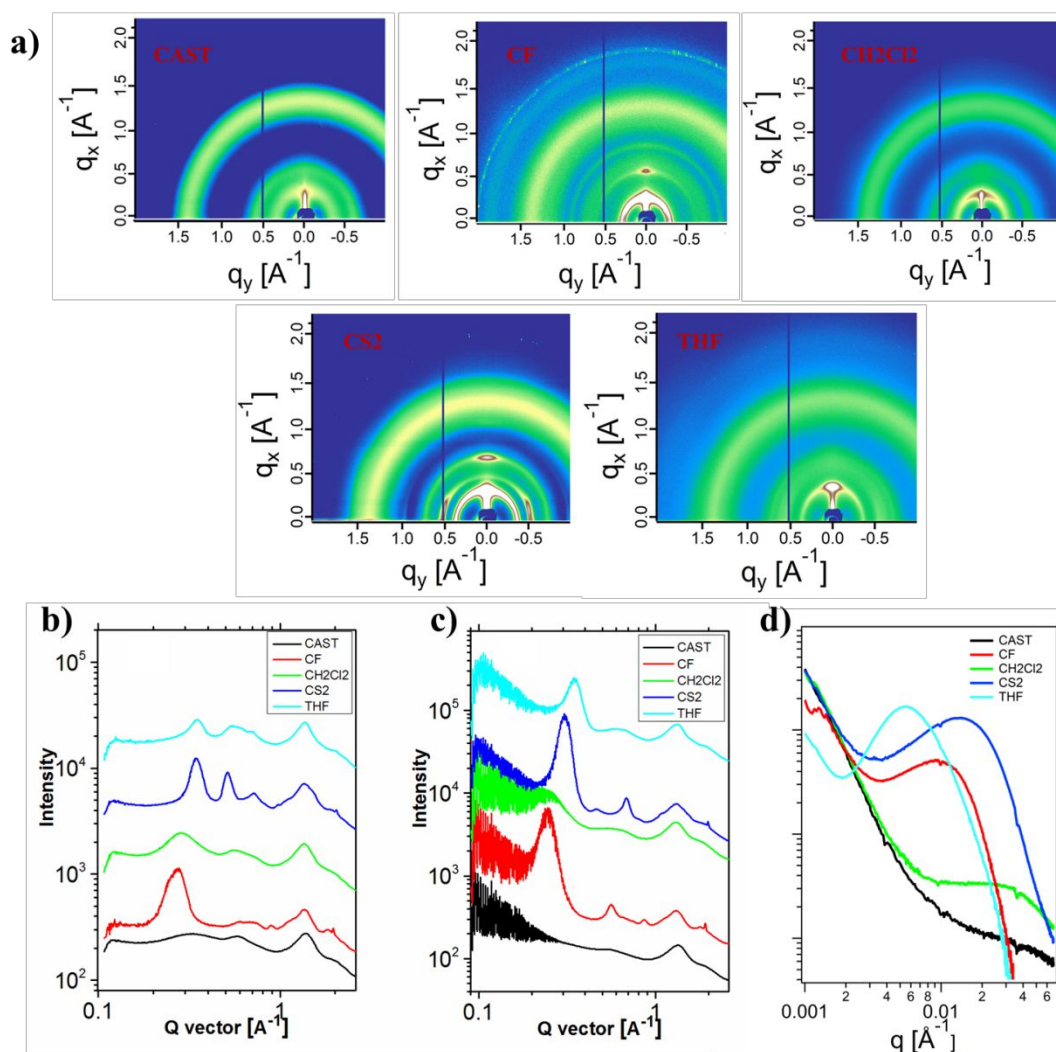
Figure 4. a) Diffraction patterns, b) in plane and c) out of plane of GIWAXS; d) RSoXS of blend films under different solvent vapor annealing processing conditions.

Furthermore, we used the Grazing incidence wide-angle X-ray scattering (GIWAXS) to investigate crystallinity and molecular packing of the films. Figure 4a are the diffraction patterns of the blend films under different SVA treatments. Also, the corresponding profiles of in plane and out of plane line-cut are summarized in Figure 4b and 4c. Broad diffraction rings at 1.3-1.5 Å^{-1} are seen in the diffraction patterns, which come from the combination of ZnP2-DPP intermolecular π-π stacking and PC$_{61}$BM diffraction. However, it is difficult to further analyze due to the obvious overlaps of these two features. For the as-cast film, there is no obvious peaks in the q

region from 0.2 to 0.4 $Å^{-1}$, indicating the poor crystallinity and structure order in the (100) direction. After SVA treatments, the molecules become ordered in the (100) direction, And good crystal order for both CF and CS_2 treated films is seen in this direction, which is also evidenced by the sharp peaks in the out of plane direction (Fig. 4c). There is also a subtle shift in the position of (100) peak from 0.31 $Å^{-1}$ in the CS_2 treated film to 0.25 $Å^{-1}$ in the CF treated film, indicating a smaller d-spacing of 2 nm in the CS_2 treated films. The crystal coherence length (CCL) in the (100) direction for CS_2 treated film is 10.8 nm, which is slightly larger than that in the CF treated film according to the Scherrer analysis.[55] Therefore, the CS_2 treated films exhibit a higher degree of molecular order, as proved by a tighter molecular packing, larger crystal coherence length and even the appeared (200) reflection peak. However, for the CH_2Cl_2 treated film, a broad peak in blend spectrum indicated that the ZnP2-DPP crystals are smaller than those in CF and CS_2 treated film.

And the phase separation of these blend films were investigated by using resonant soft X-ray scattering (RSoXS). Shown in Figure 4d are the scattering profiles of the five blend films under the different processing conditions. No obvious peak and very low scattering intensities for the as-cast film suggest the lack of phase separation due to the well-mix of ZnP2-DPP with $PC_{61}BM$ mediated by pyridine leading to severe bimolecular combination and therefore an extremely low FF for the corresponding solar cell devices. For the CH_2Cl_2 treated film, a broad hump in the regions from 0.01 to 0.06 $Å^{-1}$ is seen, indicating that there is a continuous length scale of phase separation from 10 nm to 60 nm in this film. However, the low scattering intensity suggests the weak degree of phase separation, and as results, the corresponding devices exhibit moderate FF and J_{SC} values. For the THF treated film, the peak is at 0.005 $Å^{-1}$, and the corresponding length scale of phase separation is about 125 nm, which is consistent with the TEM image that serious $PC_{61}BM$ aggregations exist in the film. A large number of excitons are recombined before diffusion to the interfaces, which is responsible for the low J_{SC} of 9.47 mA cm^{-2}. On the other hand, the separation length scales are 40 and 50 nm for the CS_2 and the CF treated films, respectively. Appropriate phase separation scale is beneficial for the

solar cell devices obtain high J_{SC}. Furthermore, the CS_2 treated film shows a higher scattering intensity and a better phase purity. These collective morphological features correlate well with the champion J_{SC}, FF and PCE for the CS_2 treated devices.

Conclusion

In conclusion, we fabricated the solar cells based on ZnP2-DPP:$PC_{61}BM$ blend films treated by a series of low boiling solvents and tested their photovoltaic efficiencies. Notably, a remarkable PCE of 9.47% with a high FF of 69.14% for CS_2 treated device was achieved because CS_2 vapor reorganized ZnP2-DPP molecules and enhanced the J-aggregations of ZnP2-DPP, thereby increasing the crystallinity of the small molecules and forming favorable film morphology with fiber-like structure. Meanwhile, the enhanced J-aggregation of ZnP2-DPP molecule lead to enhanced absorption, photoelectric response and carrier transportation, which contributed to the very high J_{SC} of 21.40 mA/cm² of the solar cell device. The as-cast film shows a lack of phase separation due to the well-mixed blend of ZnP2-DPP and $PC_{61}BM$. Severe recombination and limited carrier transport resulted in low J_{SC} and FF, and thus an extremely low PCE of 1.70%. This result verified that suitable SVA process is very important toward achieving high PCEs of small molecule solar cells.

Acknowledgements

N00014-17-1-2241.

References

1.   C. F. Shih, T. Zhang, J. H. Li and C. L. Bai, *Joule*, 2018, **2**, 1925-1949.

2.   H. Mao, J. Xu, Y. Hu, Y. Huang and Y. Song, *J Mater Chem A*, 2015, **3**, 11976-11984.

3.   S. Chu, Y. Cui and N. Liu, *Nat Mater*, 2017, **16**, 16-22.

4.   H. Mao, X. Chen, R. Huang, M. Chen, R. Yang, P. Lan, M. Zhou, F. Zhang, Y. Yang and X. Zhou, *Sci Rep-Uk*, 2018, **8**, 9501-9510.

5.   Q. Kang, L. Ye, B. Xu, C. An, S. J. Stuard, S. Zhang, H. Yao, H. Ade and J. Hou, *Joule*, 2019, **3**, 227-239.

6.   D. Baran, R. S. Ashraf, D. A. Hanifi, M. Abdelsamie, N. Gasparini, J. A. Röhr, S. Holliday, A. Wadsworth, S. Lockett, M. Neophytou, C. J. M. Emmott, J. Nelson, C. J. Brabec, A. Amassian, A. Salleo, T. Kirchartz, J. R. Durrant and I. McCulloch, *Nat Mater*, 2016, **16**, 363-369.

7.   X. Du, T. Heumueller, W. Gruber, A. Classen, T. Unruh, N. Li and C. J. Brabec, *Joule*, 2019, **3**, 215-226.

8.   L. G. Xiao, B. He, Q. Hu, L. Maserati, Y. Zhao, B. Yang, M. A. Kolaczkowski, C. L. Anderson, N. J. Borys, L. M. Klivansky, T. L. Chen, A. M. Schwartzberg, T. P. Russell, Y. Cao, X. B. Peng and Y. Liu, *Joule*, 2018, **2**, 2154-2166.

9.   S. D. Collins, N. A. Ran, M. C. Heiber and T. Q. Nguyen, *Adv Energy Mater*, 2017, **7**, 1602242-1602287.

10.   Q. Wu, D. Deng, K. Lu and Z. X. Wei, *Chinese Chem Lett*, 2017, **28**, 2065-2077.

11.   L. G. Xiao, H. D. Wang, K. Gao, L. S. Li, C. Liu, X. B. Peng, W. Y. Wong, W. K. Wong and X. J. Zhu, *Chem-Asian J*, 2015, **10**, 1513-1518.

12.   T. S. van der Poll, J. A. Love, T. Q. Nguyen and G. C. Bazan, *Adv Mater*, 2012, **24**, 3646-3649.

13.   J. H. Wan, X. P. Xu, G. J. Zhang, Y. Li, K. Feng and Q. Peng, *Energ Environ Sci*, 2017, **10**, 1739-1745.

14.   D. Deng, Y. J. Zhang, J. Q. Zhang, Z. Y. Wang, L. Y. Zhu, J. Fang, B. Z. Xia, Z. Wang, K. Lu, W. Ma and Z. X. Wei, *Nat Commun*, 2016, **7**, 13740-13748.

15.   B. Kan, M. M. Li, Q. Zhang, F. Liu, X. J. Wan, Y. C. Wang, W. Ni, G. K. Long, X. Yang, H. R. Feng, Y. Zuo, M. T. Zhang, F. Huang, Y. Cao, T. P. Russell and Y. S. Chen, *J Am Chem Soc*, 2015, **137**, 3886-3893.

16.   L. G. Xiao, T. Q. Lai, X. Liu, F. Liu, T. P. Russell, Y. Liu, F. Huang, X. B. Peng and Y. Cao, *J Mater Chem A*, 2018, **6**, 18469-18478.

17.   H. J. Bin, J. Yao, Y. K. Yang, I. Angunawela, C. K. Sun, L. Gao, L. Ye, B. B. Qiu, L. W. Xue, C. H. Zhu, C. H. Yang, Z. G. Zhang, H. Ade and Y. F. Li, *Adv Mater*, 2018, **30**, 1706361-1706368.

18.   Y. M. Sun, G. C. Welch, W. L. Leong, C. J. Takacs, G. C. Bazan and A. J. Heeger, *Nat Mater*, 2012, **11**, 44-48.

19.   J. L. Wang, K. K. Liu, J. Yan, Z. Wu, F. Liu, F. Xiao, Z. F. Chang, H. B. Wu, Y. Cao and T. P. Russell, *J Am Chem Soc*, 2016, **138**, 7687-7697.

20. M. M. Li, F. Liu, X. J. Wan, W. Ni, B. Kan, H. R. Feng, Q. Zhang, X. Yang, Y. C. Wang, Y. M. Zhang, Y. Shen, T. P. Russell and Y. S. Chen, *Adv Mater*, 2015, **27**, 6296-6302.

21. J. Min, X. C. Jiao, V. Sgobba, B. Kan, T. Heumuller, S. Rechberger, E. Spiecker, D. M. Guldi, X. J. Wan, Y. S. Chen, H. Ade and C. J. Brabec, *Nano Energy*, 2016, **28**, 241-249.

22. J. Min, X. Jiao, I. Ata, A. Osvet, T. Ameri, P. Bäuerle, H. Ade and C. J. Brabec, *Adv Energy Mater*, 2016, **6**, 1502579-1502587.

23. K. Gao, W. Y. Deng, L. G. Xiao, Q. Hu, Y. Y. Kan, X. B. Chen, C. Wang, F. Huang, J. B. Peng, H. B. Wu, X. B. Peng, Y. Cao, T. P. Russelle and F. Liu, *Nano Energy*, 2016, **30**, 639-648.

24. F. C. Spano and C. Silva, *Annu Rev Phys Chem*, 2014, **65**, 477-500.

25. W. Li, M. Chen, J. Cai, E. L. K. Spooner, H. Zhang, R. S. Gurney, D. Liu, Z. Xiao, D. G. Lidzey, L. Ding and T. Wang, *Joule*, 2019, **3**, 819-833.

26. B. G. Kim, K. Chung and J. Kim, *Chem-Eur J*, 2013, **19**, 5220-5230.

27. B. K. An, S. K. Kwon, S. D. Jung and S. Y. Park, *J Am Chem Soc*, 2002, **124**, 14410-14415.

28. G. Chen, H. Sasabe, W. Lu, X. F. Wang, J. Kido, Z. R. Hong and Y. Yang, *J Mater Chem C*, 2013, **1**, 6547-6552.

29. J. D. Zimmerman, V. V. Diev, K. Hanson, R. R. Lunt, E. K. Yu, M. E. Thompson and S. R. Forrest, *Adv Mater*, 2010, **22**, 2780-2783.

30. L. G. Xiao, S. Chen, X. B. Chen, X. B. Peng, Y. Cao and X. J. Zhu, *J Mater Chem C*, 2018, **6**, 3341-3345.

31. V. Cuesta, R. Singhal, P. de la Cruz, G. D. Sharma and F. Langa, *Acs Appl Mater Inter*, 2019, **11**, 7216-7225.

32. K. Gao, L. S. Li, T. Q. Lai, L. G. Xiao, Y. Huang, F. Huang, J. B. Peng, Y. Cao, F. Liu, T. P. Russell, R. A. J. Janssen and X. B. Peng, *J Am Chem Soc*, 2015, **137**, 7282-7285.

33. T. X. Liang, L. A. Xiao, K. Gao, W. Z. Xu, X. B. Peng and Y. Cao, *Acs Appl Mater Inter*, 2017, **9**, 7131-7138.

34. S. Chen, L. Yan, L. G. Xiao, K. Gao, W. Tang, C. Wang, C. H. Zhu, X. Z. Wang, F. Liu, X. B. Peng, W. K. Wong and X. J. Zhu, *J Mater Chem A*, 2017, **5**, 25460-25468.

35. T. Q. Lai, X. B. Chen, L. G. Xiao, L. Zhang, T. X. Liang, X. B. Peng and Y. Cao, *Chem Commun*, 2017, **53**, 5113-5116.

36. A. D. Zhang, C. Li, F. Yang, J. Q. Zhang, Z. H. Wang, Z. X. Wei and W. W. Li, *Angew Chem Int Edit*, 2017, **56**, 2694-2698.

37. Q. Q. Zhang, X. P. Xu, S. Chen, G. B. Bodedla, M. Z. Sun, Q. Hu, Q. Peng, B. L. Huang, H. Z. Ke, F. Liu, T. P. Russell and X. J. Zhu, *Sustain Energ Fuels*, 2018, **2**, 2616-2624.

38. W. T. Hadmojo, D. Yim, S. Sinaga, W. Lee, D. Y. Ryu, W. D. Jang, I. H. Jung and S. Y. Jang, *Acs Sustain Chem Eng*, 2018, **6**, 5306-5313.

39. W. T. Hadmojo, U. H. Lee, D. Yim, H. W. Kim, W. D. Jang, S. C. Yoon, I. H. Jung and S. Y. Jang, *Acs Appl Mater Inter*, 2018, **10**, 41344-41349.

40. Y. T. Guo, A. D. Zhang, C. Li, W. W. Li and D. B. Zhu, *Chinese Chem Lett*, 2018, **29**, 371-373.

41. L. L. Xu, C. L. Ho, L. Liu and W. Y. Wong, *Coordin Chem Rev*, 2018, **373**, 233-257.

42. L. G. Xiao, T. X. Liang, K. Gao, T. Q. Lai, X. B. Chen, F. Liu, T. P. Russell, F. Huang, X. B. Peng and Y. Cao, *Acs Appl Mater Inter*, 2017, **9**, 29917-29923.

43. L. G. Xiao, K. Gao, Y. D. Zhang, X. B. Chen, L. T. Hou, Y. Cao and X. B. Peng, *J Mater*

Chem A, 2016, **4**, 5288-5293.

44.   W. Keawsongsaeng, J. Gasiorowski, P. Denk, K. Oppelt, D. H. Apaydin, R. Rojanathanes, K. Hingerl, M. Scharber, N. S. Sariciftci and P. Thamyongkit, *Adv Energy Mater*, 2016, **6**, 1600957-1600967.

45.   M. Vartanian, P. de la Cruz, S. Biswas, G. D. Sharma and F. Langa, *Nanoscale*, 2018, **10**, 12100-12108.

46.   V. Piradi, X. P. Xu, Z. Y. Wang, J. Ali, Q. Peng, F. Liu and X. J. Zhu, *Acs Appl Mater Inter*, 2019, **11**, 6283-6291.

47.   M. M. Li, K. Gao, X. J. Wan, Q. Zhang, B. Kan, R. X. Xia, F. Liu, X. Yang, H. R. Feng, W. Ni, Y. C. Wang, J. J. Peng, H. T. Zhang, Z. Q. Liang, H. L. Yip, X. B. Peng, Y. Cao and Y. S. Chen, *Nat Photonics*, 2017, **11**, 85-90.

48.   K. Zhang, K. Gao, R. X. Xia, Z. H. Wu, C. Sun, J. M. Cao, L. Qian, W. Q. Li, S. Y. Liu, F. Huang, X. B. Peng, L. M. Ding, H. L. Yip and Y. Cao, *Adv Mater*, 2016, **28**, 4817-4823.

49.   T. Q. Lai, L. G. Xiao, K. Deng, T. X. Liang, X. B. Chen, X. B. Peng and Y. Cao, *Acs Appl Mater Inter*, 2018, **10**, 668-675.

50.   Z. C. Hu, K. Zhang, F. Huang and Y. Cao, *Chem Commun*, 2015, **51**, 5572-5585.

51.   F. Nuesch and M. Gratzel, *Chem Phys*, 1995, **193**, 1-17.

52.   F. Meinardi, M. Cerminara, A. Sassella, R. Bonifacio and R. Tubino, *Phys Rev Lett*, 2003, **91**, 247401-247404.

53.   P. W. M. Blom, V. D. Mihailetchi, L. J. A. Koster and D. E. Markov, *Adv Mater*, 2007, **19**, 1551-1566.

54.   L. G. Xiao, S. Chen, K. Gao, X. B. Peng, F. Liu, Y. Cao, W. Y. Wong, W. K. Wong and X. J. Zhu, *Acs Appl Mater Inter*, 2016, **8**, 30176-30183.

55.   D. M. Smilgies, *J Appl Crystallogr*, 2009, **42**, 1030-1034.

Table of Contents
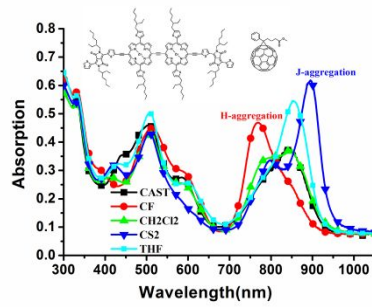
The enhanced J-aggregations increase the crystallinity of the small molecules and form favorable film morphology with fiber-like structure